Thin Solid Films, *200* (1991) 117–127
PREPARATION AND CHARACTERIZATION

LATTICE DISTORTION IN THIN FILMS OF IVB METAL (Ti, Zr, Hf) NITRIDES

I. GOLDFARB, J. PELLEG AND L. ZEVIN*
Materials Engineering Department, Ben-Gurion University of the Negev, Beer-Sheva (Israel)
N. CROITORU
Department of Electronic Devices and Materials and Electromagnetic Radiation, Tel-Aviv University (Israel)
(Received April 26, 1990; accepted November 15, 1990)

Nitride films of IVB metals (titanium, zirconium and hafnium) exhibit non-conventional lattice distortion which is displayed in the expansion of the lattice parameter calculated from the (111) diffraction peak. It is commonly assumed that this phenomenon may be explained in terms of rhombohedral distortion of the cubic lattice. However, our experimental data do not agree with the shift and broadening of the peak that are characteristic of rhombohedral distortion. We propose an alternative model for the observed expansion which is based on selective trapping of interstitial atoms in various crystallographic planes. It is shown that entrapment of interstitial atoms in the (111) plane is favorable, in comparison with the (100) plane. Entrapped atoms cause hydrostatic lattice expansion which varies with the different orientations of the grains. Non-uniform lattice expansion seems to be the main source of intrinsic microstrains and macrostrains usually observed in thin sputtered films.

1. INTRODUCTION

During the past few years there has been increasing interest in thin films of IVB metal (titanium, zirconium and hafnium) nitrides. As a consequence of their physical and chemical properties they have been considered for a wide variety of technological applications, including gate electrodes and interconnections in very-large-scale integration (VLSI), single-layer solar collectors and tribological coatings. TiN, which exhibits exceptional wear resistance and has an attractive appearance, is used as a protective coating on high-speed tools and as a decorative coating on watches and other goods.

The electrical (conductivity), optical (color) and mechanical (wear resistance, hardness) properties of nitride films depend on their composition, states of stress, and the degree of perfection of their structure. A great deal of effort has been devoted to studying the deposition process and the probable structure distortions in sputtered films of metal nitrides. Nitrides of IVB metals at compositions close to

* Also at the Institute for Applied Research, Ben-Gurion University of the Negev, Beer-Sheva (Israel).

0040-6090/91/$3.50 © Elsevier Sequoia/Printed in The Netherlands

stoichiometric exhibit an NaCl type structure with nitrogen filling the octahedral sites. It has been noted that lattice constants calculated on the bases of (200) or (311) diffraction peaks are of the same magnitude, while the (111) peak gives a significantly greater value. This phenomenon has been observed for the three nitrides, TiN[1–3] ZrN[4] and HfN[5–7], especially when the lattice parameter exceeds the value of the stoichiometric composition.

It is accepted that lattice expansion in the direction normal to a nitride film is partially due to the intake of excess nitrogen atoms and partially to Poisson expansion of the (generally) compressed film[8]. Compressive strains in nitride films also result from constrained lattice expansion due to atom shot peening and other similar effects. Thus, excessive expansion of the lattice in the [111] direction may be regarded as the outcome of numerous point defects, such as excess nitrogen, argon, or other components present in the plasma. It has been supposed by several workers[6,7] that the increased (111) spacing is the result of rhombohedral distortion of the cubic lattice, which might occur through some kind of ordering of nitrogen, metal atoms or vacancies. However, ordering seems to be improbable and even contradictory at the non-equilibrium condition of reactive sputtering deposition. Moreover, chaos rather than ordering might be expected during this process. Valvoda *et al.*[9] noted that lattice expansion in the [111] direction is connected to its intrinsic structure in comparison with, say, the (100) layer.

In this paper we attempt to present a plausible interpretation of the non-uniform lattice expansion on the basis of crystallographic insight into the process of film growth. We believe that this effect is closely related to the development of microstrains and macrostrains in deposited films, and thus to the physical properties of the film.

2. EXPERIMENTAL DETAILS

Reactive sputtering (MRC plasma system, model SEM-8620) was used to produce TiN and ZrN coatings on flat glass substrates which had been ultrasonically precleaned in trichloroethylene, acetone and finally ethyl alcohol. Prior to sputtering, the system was alternately evacuated and flushed several times with high-purity argon (99.999%) before being evacuated to 1.3×10^{-4} Pa. The target was presputtered for 30 min in order to remove contaminants. To improve adhesion to the substrate, a 15 min plasma etching of the substrate in $Ar–N_2$ or in pure electronic grade N_2 was performed. In addition, a titanium wire, acting as a getter, was inserted into the chamber and heated in order to improve the vacuum to a level of 9×10^{-5} Pa.

Deposition was carried out in an $N_2–Ar$ mixture of varying ratios (5%–40% N_2) at a working pressure of $(3–8) \times 10^{-1}$ Pa. The r.f. power was varied from 600 to 1100 W. The target-to-substrate distance was varied between 0.055 and 0.075 m. In addition, substrates heated up to 573 K were used, and the influence of the substrate bias on the growing film was also investigated.

Structural details of the deposited films were obtained by X-ray diffraction using a conventional Phillips diffractometer with nickel-filtered Cu Kα radiation. Data acquisition and processing included the following steps: (1) step-scanning of

the coated and non-coated sides of the specimen (steps of 0.02° or 0.05° with 10–40 s per step); (2) computer-aided background subtraction; (3) peak location by parabolic approximation of the top part of the peak; (4) measurements of peak width and determination of the centroid position. In order to account for probable systematic errors in diffractometric measurements, NBS silicon powder was used as the standard reference material. A small amount of fine powder was dusted through a 200-mesh sieve onto the surface of the specimen. Scattering angles of TiN and ZrN were corrected according to the adjacent diffraction peak of the silicon standard. The only uncertainty in this correction technique is the difference in levels of the surfaces of the specimen and the thin powder layer. However, for powder grains of approximately 30×10^{-6} m, the error does not exceed 0.01°–0.02° in 2θ.

Film composition was analyzed by Auger electron spectroscopy (AES) (Physical Electronics 549 ESCA Auger system). Depth profiling was performed by continuous argon sputtering in the AES chamber. Stoichiometric ZrN powder ("Cerac") was used for calibration.

Annealing was performed either in an argon atmosphere or in vacuum (Lindberg heavy duty furnace). In the first case the furnace chamber was repeatedly evacuated and flushed with argon, and finally an argon pressure of 0.3 MPa was maintained. In the second case the procedure was similar, but after filling with argon the chamber was again evacuated to a level of 6.7×10^{-6} Pa before introduction of the specimen from the cold region of the furnace to the hot interior. This technique was adopted since film oxidation took place at 823 K.

3. RESULTS

The results of X-ray diffraction measurements together with some deposition parameters for a ZrN film are shown in Table I. The probable deviation of a values, including systematic and random errors, does not exceed 2×10^{-13} m. The lattice constant for the stoichiometric 1:1 composition is $a = 4.5776 \times 10^{-10}$ m [10]. All the a values given in Table I exceed the stoichiometric value. The lattice constant calculated by the (111) peak is extraordinarily large, thus confirming the existence of some kind of lattice distortion. The lattice parameters for TiN films are shown in Table II. Although some samples of TiN films have expanded parameters when calculated by the (111) peak, it seems that this phenomenon is not as common in TiN films as it is in ZrN films. The stoichiometric parameter for TiN is $a = 4.2417 \times 10^{-10}$ m [11] and values close to this were obtained from all diffraction peaks. The peak widths for two ZrN samples are presented in Table III, and peak profiles for ZrN (sample 30) are shown in Fig. 1. Instrumental broadening measured with standard silicon powder is approximately 0.12° at the angle corresponding to the (111) ZrN peak. We did not attempt to separate the α_1–α_2 doublet at higher scattering angles. For the (311) peak, instrumental broadening may be equivalent to the α_1–α_2 angular distance, being equal to approximately 0.20°. Instrumental broadening for the remaining peaks lies between these two values, *i.e.* 0.12° and 0.20°. A typical depth profile of a ZrN film is shown in Fig. 2. Excluding the top layer of the film (approximately 500×10^{-10} m thick), the film composition is homogeneous. Two important features should be noted: nitrogen overstoichiometry and a

TABLE I
THE LATTICE PARAMETERS OF ZrN FILMS

Sample	*Percentage N_2 in gas* (vol.%)	*Deposition rate* ($\times 10^{10}$ m min^{-1})	*Thickness* ($\times 10^{10}$ m)	*Lattice parameters* ($\times 10^{10}$ m)			
				(111)	*(200)*	*(220)*	*(311)*
20	10	74	13300	4.625	4.613	4.600	—
24	10	75	9000	4.647	4.625	—	—
22	15	86	10300	4.669	4.649	4.607	4.604
23	15	—	7000	4.657	4.603	4.596	—
30	15	83	10000	4.629	4.588	—	4.596
31[a]	15	113	17000	4.637	4.616	4.598	4.582
32	15	—	—	4.627	4.606	—	—
33	15	38	4500	4.648	4.591	—	—
16[b]	20	—	—	4.632	4.607	4.600	—
19	20	69	11000	4.646	4.608	—	—

* Temperature 523 K [a] Temperature 573 K. [b] Temperature 523 K.

TABLE II
THE LATTICE PARAMETERS OF TiN FILMS

Sample	*Percentage N_2 in gas* (vol.%)	*Deposition rate* ($\times 10^{10}$ m/min^{-1})	*Thickness* ($\times 10^{10}$ m)	*Lattice parameters* ($\times 10^{10}$ m)			
				(111)	*(200)*	*(220)*	*(311)*
18	15	50	7700	4.247	4.254	4.259	4.253
30.1	20	—	—	4.300	4.240	—	—
30.1[a]	20	—	—	4.250	4.220	4.230	—
17	25	70	11000	4.242	4.245	4.246	4.247

[a] Annealed at 773 K for 1 h.

TABLE III
FULL HALF HEIGHT WIDTHS (FHHW) OF ZrN DIFFRACTION PEAKS

Sample	*FHHW* (deg)			
	(111)	*(200)*	*(220)*	*(311)*
19	1.35	1.60	1.80	2.60
30	1.05	1.00	1.70	1.95

significant level of carbon abundance. All the ZrN samples investigated in this study showed a similar distribution of the elements. Argon was not detected by AES in the film before argon sputtering in the AES chamber.

4. RHOMBOHEDRAL DISTORTION

The cubic lattice is distorted to rhombohedral by expansion or contraction in one of the [111] directions. Numerous examples of this type of distortion are found

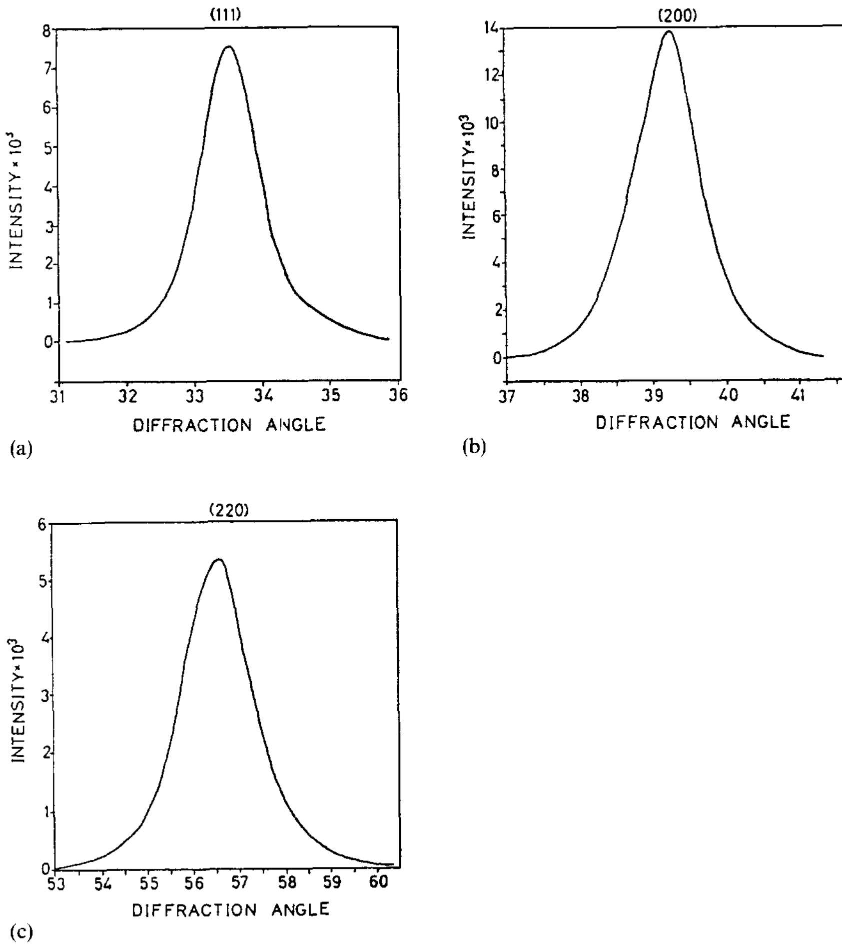

Fig. 1. Illustrative diffraction peak profiles for ZrN film (sample 30).

in ordered alloys, such as CuPd. The change of the symmetry group is reflected in the diffraction pattern. Rhombohedral distortion might be characterized by $\Delta = 90° - \alpha$, where α is the rhombohedral angle. If Δ is small ($\cos\alpha \approx \Delta$ and $\sin\alpha \approx 1$), the general expression for the d spacing of the rhombohedral lattice[12] is easily transformed to:

$$d = a/[(h^2+k^2+l^2)(-2hk+kl+hl)\Delta]^{1/2} \tag{1}$$

If d_0 and $2\theta_0$ are the d spacing and scattering angle respectively for a non-distorted cubic lattice, then the corresponding values for a rhombohedral lattice are:

$$d = d_0\{1+\Delta(hk+kl+hl)/(h^2+k^2+l^2)\} \tag{2a}$$

$$2\theta = 2\theta_0 - 2\Delta[(hk+kl+hl)/(h^2+k^2+l^2)]t\delta\theta \tag{2b}$$

The diffraction pattern of a rhombohedrally distorted ZrN crystal relative to the

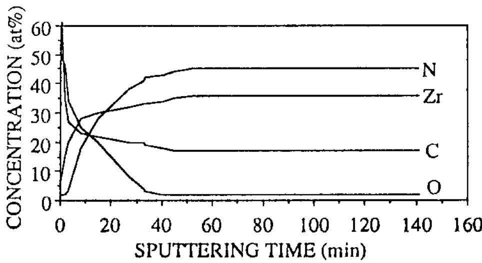

Fig. 2. AES profile for ZrN film (sample 30).

cubic is shown schematically in Fig. 3. The intensity of the split components in the cluster is proportional to the corresponding multiplicity factor, and the shift from the position of the cubic peak is given by:

$$\Delta 2\theta = -2\Delta[(hk+kl+hl)/(h^2+k^2+l^2)]t\delta\theta \tag{3}$$

The prominent features of this pattern are the constant shape of the (200) peak, the symmetrical splitting of the (220) peak, and the asymmetrical splitting of the (111) and (311) peaks. However, even for an asymmetrical cluster (111, 311, etc.), the centroids of the cluster are invariant, *i.e.* they correspond exactly to the scattering angle 2θ of a cubic lattice. This fact is especially important in analyzing non-resolved or poorly resolved clusters. An analysis of our diffraction pattern exhibiting expanded d spacings does not reveal the special features illustrated in Fig. 3. There were no visible signs of peak splitting or systematic variations of peak broadening with hkl indices (Fig. 1). Centroids were calculated for the (111), (200) and (220) peaks of a ZrN film (sample 30) and are listed in Table IV. Lattice constants calculated by centroid positions are not consistent with a cubic lattice, and the observed lattice distortion cannot be attributed to a rhombohedral type.

Some peak splitting has been observed by Johansson *et al.*[7] for HfN films. However, the nature of the splitting does not correspond to the expected situation, as shown in Fig. 3. For example, the (220) cluster is asymmetrical and a strong component of the (111) cluster is at the wrong low-angle side. The lattice constant calculated from the centroids of (111), (220) and (311) peaks are 4.86×10^{-10}, 4.513×10^{-10} and 4.53×10^{-10} m, *i.e.* values which are not consistent with a cubic lattice. Thus, the rhombohedral distortion of the cubic lattice, as suggested by Johansson *et al.* is doubtful.

Crystallographic analysis for the likelihood of rhombohedral distortion only confirms its low probability. For achieving rhombohedral distortion, ordering of atoms or vacancies is required in one of the $\langle 111\rangle$ directions, but for some of the grain orientations, such as (111) and (100), none of the $\langle 111\rangle$ directions is found in the plane of the film. Thus, ordering, if it does occur, must take place in adjacent atom layers, rather than in the given layer itself. For example, in a $\{111\}$ oriented grain, one of the probable ordering directions might be $\langle 111\rangle$, *i.e.* normal to the plane. In this case, the pattern of the occupied and vacant sites in one layer must be repeated in the subsequent deposited layers. If, however, the angle between the ordering direction and the film plane differs from 90°, then the shift of similar

TABLE IV

CENTROIDS OF DIFFRACTION PEAKS AND LATTICE CONSTANTS FOR ZrN FILM

hkl	2θ (deg)	a (Å)
(111)	33.593	4.623
(200)	39.193	4.598
(220)	56.558	4.603

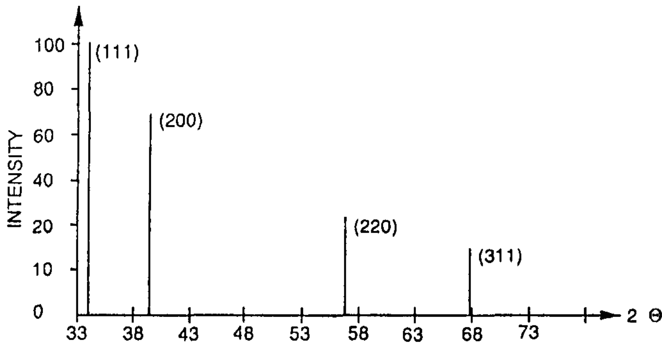

(a)

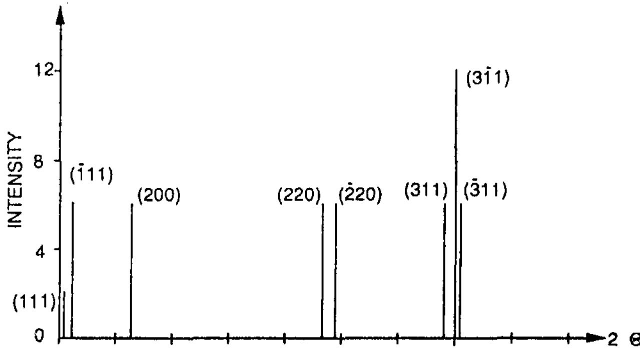

(b)

Fig. 3. Schematic diffraction patterns for ZrN: (a) cubic lattice, (b) rhombohedrally distorted lattice.

patterns of distributions of atoms and/or vacancies in adjacent layers must have a component parallel to the film plane. Such sophisticated ordering schemes, which are different for various grain orientations, can be achieved in film growth under equilibrium conditions. Such a phenomenon is very improbable during the growth of sputter-deposited nitride films.

5. SELECTIVE INTAKE OF INTERSTITIAL ATOMS

We believe, as do many other workers, that the exceptionally large expansion of the (111) spacings in nitrides is associated with an intake of excess interstitial atoms

such as nitrogen, argon etc. However, we believe this process to be direction dependent and to be more effective for (111) oriented grains than for grains with other orientations. At the outset it should be stated that although the volume density of interstitial sites is equal for all grain orientations, the surface density is the greatest for the (111) layer. Although this fact is important in the light of layer by layer growth of the nitride film, it seems that the morphology of the corresponding metal layers is of greater significance. Figures 4(a) and (b) illustrate respectively the positions of the tetrahedral and octahedral sites in the (111) and (100) layers of metal atoms. The straight lines indicate the planar unit cell for these layers. The areas of cells are $(a^2\sqrt{3})/4$ and a^2 for the (111) and (100) planes respectively. In the (111) layer each metal atom is surrounded by six voids. The final shape of the voids depends on the position of the metal atoms in the adjacent layers. One kind of void (T_1) will be a tretrahedral and the other (O) will be an octahedral site. The surface density of each of these, the T_1 or O types is equal to $4/(a^2\sqrt{3})$. Another type of tetrahedral site T_2 is formed by one metal atom of the first layer as the apex of the tetrahedron and three additional metal atoms of the adjacent layer. The surface density of the T_2 sites is also 4 $(a^2\sqrt{3})$, bringing the total density of the T sites to $8/(a^2\sqrt{3})$, *i.e.* twice the density of the octahedral sites. The elevation of the interstitial sites above the plane of metal atoms is given in Table V. T_1 sites are the deepest. It should be emphasized that the T_1 and O sites are indistinguishable before deposition of the second metal layer. There is a probability that not only O sites but also T_1 sites will be occupied, at least partially, by nitrogen or other interstitial atoms. The process is facilitated by the substantial kinetic energy (tens of electronvolts) of the impinging atoms. It is also favored when subsequent metal layer formation occurs at high enough rates so that there is not enough time for a buried atom to move to equilibrium interstitial sites. The result of such a process manifests itself in lattice expansion, which is hydrostatic in nature.

TABLE V
RELATIVE ELEVATION OF INTERSTITIALS OVER LAYER OF METAL ATOMS

Interstitials	*(111) layer*		*(100) layer*	
	Surface density	*Elevation*	*Surface density*	*Elevation*
Tetrahedral T_1	$4/\sqrt{3}a^2$	$a/4\sqrt{3}$	$4/a^2$	$a/4$
Octahedral O	$4/\sqrt{3}a^2$	$a/2\sqrt{3}$	$2/a^2$	0
Tetrahedral T_2	$4/\sqrt{3}a^2$	$3a/4\sqrt{3}$	—	—

a is the lattice parameter.

The morphology of the (100) layer is quite different. There are four T_1 sites with an elevation of $a/4$ and two O sites with zero elevation per unit cell (Fig. 4(b) and Table V). O sites in the (100) layer are almost complete and contain four metal atoms in the layer under consideration and one metal atom in the underlying layer. Only one metal atom from the incoming layer is needed to complete the octahedron. It is expected that octahedral positions in the (100) layer will be filled up first owing to the

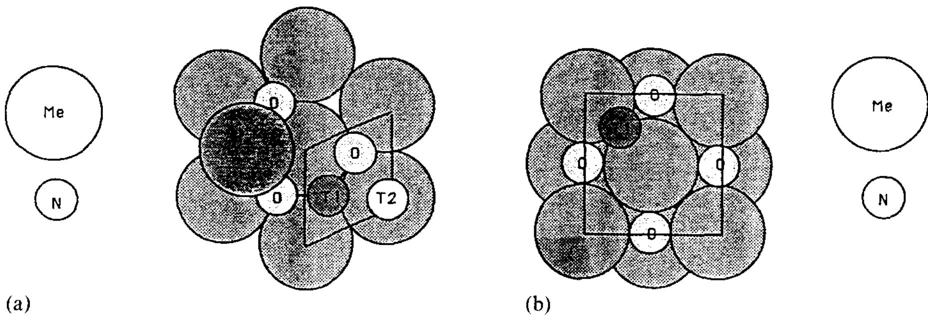

Fig. 4. Schematic drawing showing interstitials sites O, T_1, T_2 in (a) (111) and (b) (100) layers.

low elevation and near completeness of the sites. In comparison, only two of four metal atoms are available for T_1 sites, and two more have to come with the formation of the next metal layer. Moreover, a prospective occupant of a T_1 site will inevitably be subjected to strong repulsion forces from interstitial atoms already settled in the O sites. Thus, regarding the sequence of occupation in the (100) layers, it must be concluded that there is a high priority for occupation of the O sites, whereas subsequent occupation of the T_1 interstitials is highly improbable. In the case of the (111) layer the probabilities of occupation of T_1 and O sites are similar owing to the configurational similarity of the initial voids and to the lower elevation of T_1 sites in comparison with O sites. As a result, it is expected that larger lattice expansion will occur in grains with (111) orientation than in grains with (100) orientation.

The size of the T sites in the nitrides under consideration increases in the order TiN, HfN, ZrN owing to the increase in lattice constants. Although for ZrN the radius of the T site is still smaller than the radius of a nitrogen atom, it might be expected that ZrN is more susceptible to selective intake of nitrogen and other interstitial atoms by the (111) layer. This expectation is born out by our experimental results. If occupation of T sites by nitrogen or other interstitial atoms is not ordered, the lattice retains cubic symmetry, and the expansion of free-standing grains must be hydrostatic. In a dense film only the direction normal to the film is free for expansion. Compressive strains and stresses therefore develop in the plane of the film as a result of the expansion. Selective occupation of T sites in grains with various orientations is undoubtedly very important in the development of intrinsic macrostrains and microstrains in growing nitride films. The study of macrostrains is not within the scope of the present work, but microstrains may be easily evaluated by measurements of peak broadening. A typical result is shown in Fig. 5, in which $\beta\cos\theta/\lambda$ *vs.* $2\sin\theta/\lambda$ is presented (where β is the peak width). The intercept is close to $\beta\cos\theta/\lambda \approx 0$, indicating the contribution of microstrains to the total peak broadening.

6. IMPLICATIONS TO X-RAY DIFFRACTION

Our diffraction measurements, like those of the majority of other workers, were carried out with a conventional X-ray diffractometer with Bragg–Brentano

parafocusing geometry. With this geometric scheme, the diffraction vector is parallel to the film normal. In other words, the *hkl* reflecting plane must be oriented approximately parallel to the plane of the film. Thus, the (111) reflection resulted from grains with (111) orientation, which is the most favorable orientation for entrapping interstitial atoms in tetrahedral sites, will show abnormally expanded spacings. Johansson *et al.*[7] are among the few workers who used a transmission technique to study thin nitride films. Depending on the angle of incidence in their geometrical set-up and depending on the Bragg angle, reflection occurs from crystallographic planes normal (or close to normal) to the film plane. In this technique any $h_1k_1l_1$ reflection is generated by grains with different orientations $h_ik_il_i$ provided that the angle between $h_1k_1l_1$, and $h_ik_il_i$ is close to 90°. For example, grains with (111) orientation having a highly expanded lattice, grains with (001) orientation with slightly expanded lattice, and grains with any other orientation with various degrees of lattice expansions, will all contribute to the (220) reflection. The peak splitting observed by Johansson *et al.*[7] is apparently the result of overlapping reflections from grains with various degrees of lattice expansion.

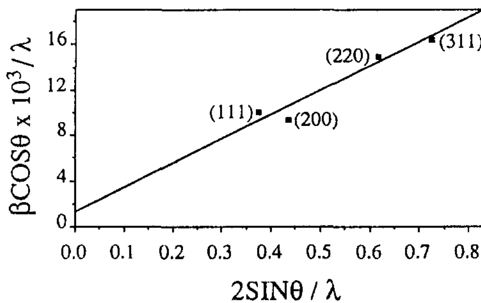

Fig. 5. Hall–Williamson plot for microstrains.

7. CONCLUSIONS

The growth of sputtered MeN films (Me ≡ Ti,Zr,Hf) takes place under highly non-equilibrium conditions. Owing to the significant kinetic energy of incoming atoms, a significant atomic shot peening occurs. Foreign atoms (argon, carbon, oxygen) as well as excess nitrogen atoms may occupy non-equilibrium positions, for example tetrahedral positions. The probability of intake of these non-stoichiometric atoms is direction dependent and is the greatest in (111) oriented grains. Thus, the concentration of non-stoichiometric atoms and lattice expansion are non-uniform in grains with different orientations, being the greatest for (111) oriented grains. This non-uniformity in polycrystalline films leads to the development of the microscopic and macroscopic strains that have been reported in numerous studies on nitride films obtained by sputtering. We believe that the grain-boundary mechanisms in the development and the relaxation of internal strains, noted by Sundgren[13] and Rickerby[14] are closely related to the proposed mechanism of film growth.

ACKNOWLEDGMENTS

A part of this work was supported by the National Council for Research and Development, Israel, under contract 25600-2-88. The support is gratefully acknowledged. One of the authors (J.P.) holds the Sam Ayerton Chair in Metallurgy.

REFERENCES

1 D. S. Rickerby, A. M. Jones and A. J. Perry, *Surf. Coatings Technol.*, *36* (1988) 631.
2 A. J. Perry, *J. Vac. Sci. Technol. A*, *4* (5) (1986) 2670.
3 J. Pelleg, L. Zevin, Sh. Lungo and N. Croitorn, *Thin Solid Films*, in the press.
4 E. O. Ristolainen, J. M. Molarius, S. Korhonen and V. K. Lindroos, *J. Vac. Sci. Technol. A*, *5* (4) (1987) 2134.
5 A. J. Perry, L. Simmen and L. Chollet, *Thin Solid Films*, *118* (1984) 271.
6 W. D. Sproul, *Thin Solid Films*, *118* (1984) 279.
7 B. O. Johansson, U. Helmersson, M. K. J. Hibbs and J. E. Sundgren, *J. Appl. Phys.*, *58* (1985) 3104.
8 Sh. Kanamori, *Thin Solid Films*, *136* (1986) 195.
9 V. Valvoda, R. Cerny, R. Kuzel, J. Musil and V. Poulek, *Thin Solid Films*, *158* (1988), 225.
10 Standard X-ray diffraction powder patterns, *National Bureau of Standards Monograph N25*, Gaithersburg, MD, 1984, p. 21.
11 Powder Diffraction File, card 38-1420, Issued by Joint Committee on Powder Diffraction Standards, Swarthmore, PA, 1989.
12 L. V. Azaroff, *Elements of X-Ray Crystallography*, McGraw Hill, New York, 1968.
13 J.-E. Sundgren, *Thin Solid Films*, *105* (1983) 367.
14 D. S. Rickerby, *J. Vac. Sci. Technol. A*, *4* (1986) 2809.